Sensitivity and Interpretation of Zonal Mean Climate from Two Atmospheric General Circulation Models with Different Dynamical Cores

He Zhang[1], Minghua Zhang[2], and Qingcun Zeng[1]

1. Institute of Atmospheric Physics, Chinese Academy of Sciences, Beijing, China

2. State University of New York at Stony Brook, Stony Brook, New York

Abstract

The dynamical cores of the fourth version of the Institute of Atmospheric Physics of Chinese Academy of Sciences atmospheric general circulation model (IAP AGCM4.0) and the Community Atmosphere Model version 3.1 (CAM3.1) are used with the same CAM3.1 physical parameterizations to study the sensitivity of the simulated zonal mean climate. Compared to NCEP reanalysis data, the IAP AGCM4.0 core reduced the CAM3.1 warm bias climate in the troposphere from above 2K to less than 1 K. The IAP model simulated a colder troposphere and weaker westerly jets that are more consistent with observations. However, when the two dynamical cores are used in the idealized Held-Suarez tests without moisture physics, the IAP AGCM core simulated a warmer troposphere than that in the CAM3.1. The causes of the differences in the full models and in the dry models are studied. We show that the IAP dynamical core has less energetic eddies, and weaker eddy transports of heat and momentum, which produced weaker residual circulations to cool the troposphere. As a result, the IAP dry model simulated a warmer troposphere. When moist physics is included, however, the diabatic heating also changes. The IAP model simulated reduced amount of high clouds thus less greenhouse effect of these clouds in the upper troposphere, leading to larger radiative cooling. The effect from the diabatic heating dominates the effect from the eddy-forced residual circulation. Therefore, the IAP model with full physics simulated a colder troposphere than the CAM3.1. This is further supported by aqua-planet experiments that included moist physics. Our results show how interactive physical processes can change the effect of a dynamical core on climate simulations.

---

1. Introduction

The IAP AGCM4.0 is the fourth version of the Institute of Atmospheric Physics (IAP) of Chinese Academy of Sciences atmospheric general circulation model developed by a model group in IAP. Its first version, IAP AGCM1.0, was designed in 1980's as the first general circulation model used for climate simulations in China (Zeng et al. 1989). IAP AGCM1.0 used a horizontal resolution of 4° latitude × 5° longitude and 2 σ layers in the vertical with the top at 200 hPa. The second and third versions of the IAP AGCM used increased model resolutions of 4°lat×5°lon×9L for IAP AGCM2.0 (Bi 1993; Liang 1996) and 2°lat×2.5°lon×21L for IAP AGCM3.0 (Zuo 2003) respectively, along with modifications in the time integration

scheme and physical parameterizations. These three versions of the IAP AGCM have been used to investigate the behavior of the earth's climate system and to predict summer precipitation anomalies and spring dust storms in China (e.g., Zeng et al. 1997; Xue et al. 2001; Chen et al. 2004). In the fourth version of the IAP AGCM, the main features of the dynamical core are inherited from the earlier versions, but new features have been introduced (details in section 2). The physical processes of the IAP AGCM4.0 however are not a simple inheritance of former versions. Instead, as an intermediate version, we adopted the full physics package of the Community Atmosphere Model version 3.1 (CAM3.1) (Collins et al. 2004). The model therefore gives us an opportunity to evaluate the impact of the IAP dynamical core on the simulated climate. New physical schemes of radiative transfer, heterogeneous cloud nucleation, convection parameterization, and a new scheme for boundary layer fluxes are currently being introduced for the next version of the model.

The objective of this paper is to investigate the sensitivity of the IAP AGCM4.0 to the dynamical core. We show that the IAP model with full physics improved the temperature and zonal winds in the CAM3.1 by simulating a colder atmosphere, but the dry version of the model simulated a warmer climate than the CAM3.1. This type of opposite sensitivities of the moist and dry models to the dynamical core has been also reported in the past in other models (Chen et al. 1997), but the cause has not been explained before. Previous studies have also reported the impact of dynamical cores on atmospheric simulations (e.g., Boer and Denis; Polvani et al. 2004; Jablonowski and Williamson 2006). To our knowledge, however, no study has investigated the different sensitivities between the dry and moist models.

This paper is organized as follows. Brief descriptions of the IAP AGCM4.0 and the experiments are given in section 2. Section 3 compares the simulations of temperature and general circulation between IAP AGCM4.0 and CAM3.1. Results from the dry model and aqua planet tests are also represented, along with diagnostics of eddy activities and interpretation in the transformed Eulerian mean framework. The last section contains a summery.

2. Model description and experimental setup

The IAP AGCM4.0 is a finite-difference model with a terrain-following σ coordinate. A latitude-longitude grid with Arakawa's C grid staggering is used for the horizontal discretization. In order to compare with CAM3.1 conveniently, the vertical levels 26 and their locations are set approximately the same as CAM3.1. There are 128 grids in latitudes and 256 grids in longitudes, which are also the same with the T85 spectral resolution of CAM3.1.

Unique features of the IAP dynamical core include the exact conservation of *available* total energy rather than total energy, subtraction of standard stratification that minimizes the large truncation errors in the mountain regions, the nonlinear iterative time integration method, and internal consistence according to physical laws (Zeng et al. 1989; Zeng and Mu 2002). New features of the IAP AGCM4.0 include the flexible leaping-point scheme at high latitude to enlarge the time step, flexible but permissible substitutions to smooth without violating energy conservation, time splitting method to economize CPU time, and introduction of dissipation term in the predictive equation for surface pressure to damp numerical noise (Zeng and Mu 2002; Zhang et al. 2009). The CAM3.1 dynamical core uses the standard spectral-transform method detailed by Collins et al. (2004).

As mentioned in the introduction, the CAM3.1 physical package described in Collins et al. (2004) is adopted in the current version IAP AGCM4.0. The IAP AGCM4.0 and CAM3.1 are both integrated for 17 years respectively with nearly the same resolutions, the same physics package, the same boundary data and the same initial conditions. Averages of simulations in the last 15 years are presented. The SST and sea ice datasets used to force the AGCMs are climatological monthly datasets from blended products that combined the global Hadley Centre Sea Ice and Sea Surface Temperature (HadISST) dataset (Rayner et al. 2003) for years up to 1981 and the Smith/Reynolds EOF dataset (Reynolds et al. 2002) post-1981. The concentrations of greenhouse gases are held constant at their levels in 1990. The primary source of the validation data is NCEP/NCAR reanalysis (Kalnay et al. 1996). Both the model results and reanalysis data are truncated to T42 for direct comparison.

3. Results

a. Temperature and general circulation from climate simulations

We have examined a suite of atmospheric fields from the IAP AGCM4.0 by using the AMWG diagnostics package (Zhang, 2009). The overall performance is similar to the CAM3.1 that was described in Hurrell et al. (2006). We therefore only focus on the differences between the simulations of the IAP AGCM4.0 and the CAM3.1.

Figures 1a and 1b show the deviation of the zonally averaged temperature from the NCEP reanalysis in the models. The differences between the IAP AGCM4.0 and the CAM3.1 simulations are shown in Figure 1c. As in most of the AGCMs (Boer et al., 1992), there exists a notable cold bias near the polar tropopause in both models. However, this cold bias in the IAP AGCM4.0 is about 2K smaller than in the CAM3.1 in the Sorthern Hemisphere (SH). Moreover, the CAM3.1 has a warm bias throughout most of the troposphere. This warm bias is systematically reduced in the IAP AGCM4.0, especially in the tropical and subtropical regions between 30°N and 30°S, where the simulated temperature in the IAP AGCM4.0 is colder than that in the CAM3.1 by 1-2 K.

Distribution of zonal wind has traditionally been one of the fundamental measures of climate simulations. It is closely linked geostrophically to the temperature by thermal wind relation. Figures 2a to 2c show that both models simulated the main features of the observed zonal winds, including the westerly jet cores located near 200 hPa over the middle-latitudes of both hemispheres, and the tropical easterlies in the lower and middle troposphere as well as in the stratosphere. The two models all overestimated the intensity of the westerly jet in both hemispheres (Figures 2d and 2e). This overestimation however is reduced by about half in the IAP AGCM4.0 relative to the CAM3.1. The jets in the CAM3.1 are stronger than in the NCEP/NCAR reanalysis by 4-6 m s^{-1} and 6-8 m s^{-1} in Northern Hemisphere (NH) and SH respectively, while the corresponding biases in the IAP AGCM4.0 are about 2 m s^{-1} and 4 m s^{-1}. This can be more clearly seen in the difference figure between the two models (Figure 2f). Besides the strength, the locations of the jets are also different. The jet simulated in the IAP AGCM4.0 has a slight equatorward shift relative to that in the CAM3.1(Figures 2b and 2f), which may be mainly explained by the smaller meridional temperature gradient (Figure 1c) according to the thermal wind relationship. Furthermore, the relative heating above tropopause in tropical region

(Figure 1c) can also contribute the equatorward shift of the jet in the IAP AGCM4.0 (Lorenz and DeWeaver, 2007).

Transports of heat and momentum by eddies are important mechanisms to establish the general circulation and maintain the energy balance as well as angular momentum conservation of the atmosphere. The simulated zonally averaged transient heat fluxes with the IAP AGCM4.0 and the CAM3.1, which constitute the bulk of the total heat fluxes in the models, and their differences are shown in Figures 3. While the models show significant similarities, with two peaks of poleward heat fluxes in the lower and upper tropospheres, there are two notable differences. Above 500 hPa, the poleward heat transport is weaker in the IAP model; below 500 hPa, there is a shift of the transport pattern to lower latitudes.

The weaker poleward heat transport in the upper troposphere in the IAP model is the result of weaker eddy activities. This can be seen in the eddy momentum transport of Figures 4. Previous studies have also shown large sensitivities of eddy kinetic energy to dynamical cores (Wan et al. 2008). Therefore, the difference in the upper troposphere can be attributed to the finite difference scheme that is more diffusive in the IAP AGCM4.0 than in the CAM3.1. The difference in the lower troposphere in the heat transport, as will be shown later, is is likely related to the colder troposphere in the IAP model..

b. Held-Suarez test

To understand the above differences between the two models, we carried out idealized dry-model experiments proposed by Held and Suarez (1994), hereafter referred to as H-S. Specified forcing is used in the thermodynamic and momentum equations to yield a circulation that is grossly similar to the observation in the troposphere. The thermal forcing is Newtonian relaxation to a specified temperature field of varying time scale with latitudes and pressure. The momentum forcing is a sink represented by Rayleigh friction in the lower troposphere. The atmosphere is integrated without moist processes, topography, land-sea contrast and seasonal or diurnal cycle.

The initial data is not important in the H-S test, since after a certain period of integration, the prescribed forcing drives the model dynamics to quasi-equilibrium state that is independent of the initial state. In this paper, the integration of the IAP AGCM4.0 dynamical core (hereafter IAP core) started from the same initial data as for the full model run. The CAM3.1 dynamical core (hereafter CAM core) was integrated from an earlier run of a lower resolution T42 to avoid the computational instability caused by disequilibrium between wind and pressure gradient due to lack of topography. As proposed by Held and Suarez (1994), both of the two models were integrated for 1200 days, and the time-mean fields and statistics are taken from the last 1000 days.

Figure 5 shows zonally averaged 1000-day mean temperature from the H-S tests with the IAP core and CAM core and their difference. The major feature of the real atmosphere is reproduced with the idealized forcing, although the simulated upper atmosphere is unrealistically cold by inactive forcing in the stratosphere. The simulated troposphere in the IAP core is warmer than that in the CAM core, which is opposite to the results found in the climate simulations, except in middle latitude below 700 hPa where the IAP core is 0.5-1.5K colder than the CAM core.

As expected from the thermal wind relationship, the simulated westerly jets in the IAP core are stronger than those from the CAM core (Figure 6). This difference is also opposite to that in the climate simulations, in which the jets are weaker in the IAP AGCM4.0.

The distribution of simulated eddy heat flux from H-S tests is presented in Figure 7. The patterns of eddy heat fluxes of the H-S tests are similar to the climate simulations with two peaks located in lower and upper troposphere respectively. The difference between the two dynamical cores in Figure 7c shows that the eddy heat flux in the IAP core is weaker than the CAM core throughout the troposphere. The eddy momentum fluxes simulated by two cores are shown in Figure 8. Consistent with the full models, the values of the maximum are smaller in the IAP core. Moreover, there is a poleward shift of the maximum centers in the IAP core (Figure 8c) that is associated with the warmer troposphere.

As will be shown later, these features of the differences between the two dynamical cores can be explained by the overall weaker wave activities in the IAP core. The weaker poleward heat flux can explain why the tropospheric temperature from 30^oS to 30^oN is warmer in the IAP core in the H-S tests (fig. 7c), and colder in middle latitudes.

c. Aqua-planet test

To understand why the IAP AGCM4.0 with full physics simulated a colder troposphere relative to CAM3.1, but a warmer troposphere in the H-S test, we further conducted aqua-planet experiments to examine the possible impact of the different treatment of surface topography in the full models. Following Neale and Hoskins (2001), the full AGCM including dynamics and physics is used, but the surface boundary is drastically simplified by using a uniformly water-covered surface. The idealized control SST in Neale and Hoskins (2001) is used in this paper. The results from the aqua-planet tests by IAP AGCM4.0 (hereafter IAP aqua) and by CAM3.1 (hereafter CAM aqua) are compared with the results from real climate simulations and from H-S tests. If the results are similar with that from H-S tests, the influence by topography will be the reason of the improvement of temperature simulation in IAP AGCM4.0. On the other hand, if the results are similar with that from real climate simulations, the contribution by topography is then not important.

As in Neal and Hoskins (2001), the aqua-planet simulations by the two models are integrated for 40 months, with the last 36 months used for the analysis. For simplicity, only the differences of the two models are given here (Figure 9). Relative to the CAM aqua, the following four features can be identified: (1) the IAP aqua simulated a colder troposphere on the aqua-planet (Figure 9a); (2) the westerly jet is weaker and displaced equatorward in the IAP model (Figure 9b); (3) the polarward eddy heat transport at middle latitude around 45°N and 45°S is weaker in the IAP aqua (Figure 9c); (4) the momentum transport is weaker in the IAP model (Figure 9d). The first two features are consistent with the differences between the two models with full physics, but opposite to those in the H-S tests. The last two features are consistent among all experiments.

These results confirm that the IAP dynamical core is more diffusive, with less energetic eddies, and thus weaker poleward of heat. The cause of the difference in the temperature between the moist and dry models is therefore mostly related with the introduction of moist physics, which is further studied next.

d. Residual circulation and diabatic heating

Under steady-state conditions, the zonally averaged atmospheric thermodynamic balance is between the adiabatic cooling, the eddy forcing, and the diabatic heating:

As pointed out by Andrews and McIntyre (1976), there tends to be a strong cancellation between the convergence of eddy heat flux and the adiabatic cooling due to eddy-induced meridional circulation. Thus, it is the residual meridional circulation, after cancellation of these two terms that is more directly related to the diabatic heating. Using the transformed Eulerian mean (TEM) framework of Andrews and McIntyre (1976), the residual circulation ($\overline{v}^*$, $\overline{w}^*$) and the vector Eliassen-Palm (EP) flux **F** are defined by (see Holton, 2004)

$$\overline{v}^* = \overline{v} - \frac{R}{\rho_0 H}\frac{\partial}{\partial z}\left(\frac{\rho_0}{N^2}\overline{v'T'}\right) \tag{1}$$

$$\overline{w}^* = \overline{w} + \frac{R}{Ha\cos\varphi}\frac{\partial}{\partial \varphi}\left(\frac{\cos\varphi}{N^2}\overline{v'T'}\right) \tag{2}$$

$$\mathbf{F} = \left(F_\varphi, F_z\right) = \left(-\rho_0 a\cos\varphi\,\overline{v'u'}, \rho_0 a\cos\varphi\frac{Rf}{HN^2}\overline{v'T'}\right) \tag{3}$$

the TEM thermodynamic equations can be written as

$$\frac{\partial \overline{T}}{\partial t} = \overline{Q} - \frac{HN^2}{R}\overline{w}^* \tag{4}$$

the residual circulation is related with eddy-forcing and diabatic heating as

$$\frac{\partial}{a^2\partial\varphi}\left(\frac{1}{\cos\varphi}\frac{\partial\overline{\chi}^*}{\partial\varphi}\right) + \rho_0\frac{f^2}{N^2}\frac{\partial}{\partial z}\left(\frac{1}{\rho_0\cos\varphi}\frac{\partial\overline{\chi}^*}{\partial z}\right) = \frac{\rho_0}{N^2}\left[\frac{\partial}{a\partial\varphi}\left(\frac{R\overline{Q}}{H}\right) + f\frac{\partial\overline{G}}{\partial z}\right] \tag{5}$$

with the stream function of the residual circulation ($\overline{\chi}^*$) definition as

$$\rho_0\overline{v}^*\cos\varphi = -\frac{\partial\overline{\chi}^*}{\partial z}, \qquad \rho_0\overline{w}^*\cos\varphi = \frac{\partial\overline{\chi}^*}{a\,\partial\varphi} \tag{6}$$

where

$$\bar{G} \equiv \frac{1}{\rho_0 a \cos\varphi} \nabla \bullet \mathbf{F} + \bar{X}$$

$$N^2 = \frac{R}{H}\left(\frac{\kappa \bar{T}}{H} + \frac{\partial \bar{T}}{\partial z}\right)$$

$$z = -H \ln \frac{p}{p_0}$$

$$\rho_0 = \frac{p_0}{gH} e^{-z/H}$$

$$\kappa = \frac{R}{C_p}$$

In the above, a is the earth radius, g the gravity acceleration, R the gas constant for dry air, c_p the specific heat of dry air at constant pressure, φ the latitude, f the Coriolis parameter, u the zonal wind, v the meridional wind, w the vertical velocity, T the temperature, X the subgrid-scale momentum forcing, Q the diabatic heating, the scale height $H = 7$ km, the reference pressure $p_0 = 1000$ hPa. The bar denotes the zonal mean and the prime the deviation from the zonal mean. The EP flux is a measure of wave activities.

Figure 10a demonstrates the EP flux and its divergence in the IAP core. It can be seen that planetary waves propagate into upper troposphere from the primary source region in the lower troposphere at middle latitudes. The difference field (Figure 10b) clearly shows that these wave activities in the IAP model are weaker. Figure 11a gives the corresponding residual circulation from the IAP core. There is broad descending motion, corresponding to adiabatic warming, in middle and high latitudes that balance the diabatic cooling from the temperature relaxation, in which the model temperature is larger than the reference temperature (not shown, see Zhang et al. 2010). In low latitudes, the residual circulation is ascent, a cooling effect, which balances the diabatic warming, because the model temperature is smaller than the reference temperature.

The difference field of the residual circulation from the two dry models in Figure

11b shows overall weakening of the circulation in the IAP model, thereby reducing the upward motion equatorward of 40^{o}N and 40^{o}S. This reduces the adiabatic cooling and therefore results in a warmer troposphere.

Poleward of 40^{o}N and 40^{o}S, the difference of the residual circulation in Figure 11b corresponds to stronger upward motion in the lower troposphere in the IAP model. This explains the colder temperature difference in Figure 5c. Therefore, when compared with the CAM3.1 dry model, the weaker eddy fluxes of heat and momentum in the IAP dry model can explain the weaker residual circulation and the warmer tropospheric temperature in bulk of the troposphere.

This interpretation becomes different for the moist models. Figure 10d shows the difference of EP fluxes as a measure of the wave activities between the two moist models. The IAP model also simulated overall weaker wave activities throughout the troposphere. The change in the residual circulation in Figure 11d is however very different. In each hemisphere, the circulation is weaker in low latitudes, but stronger in middle latitudes. This lack of direct correspondence between the eddy activity and residual circulation suggests that the diabatic heating also played a major role, as discussed below.

e. Interaction between moist physics and dynamics

Equation (4) shows that under steady state conditions, the adiabatic cooling from the residual circulation should balance the diabatic heating. However, the interaction between the adiabatic cooling and the diabatic heating in dry models is different from that in moist models. In the dry models, the diabatic heating term is the relaxation to temperature, so it is passive to adiabatic cooling. While in the moist models, the interaction between diabatic heating and adiabatic cooling is so strong that we can't tell which is active and which is passive. The above conclusions can be demonstrated from Figure 12, which gives the evolution of adiabatic heating rate, diabatic heating rate and total heating rate in H-S tests with IAP dry model as well as in climate simulations with IAP moist model, respectively. The corresponding correlation coefficients of adiabatic heating, diabatic heating and total heating are given in Table 1. In H-S test, there is no significant correlation between adiabatic heating and

diabatic heating, and the total heating primarily follows on the adiabatic heating term. However, in the full mode, there is significant negative correlation between adiabatic heating and diabatic heating in climate simulation. Namely, if there is a warming due to adiabatic processes, the diabatic processes will make a quick response to cool the atmosphere. Both of adiabatic heating and diabatic heating have a significant contribution to the total heating.

The major diabatic heating considered in AGCMs includes radiative heating, vertical diffusive heating and the heating due to moist processes, such as convection. Because the vertical diffusive heating merely affects low troposphere below 850 hPa, we will not discuss it here since we focus on vertical distribution of temperature at middle and high troposphere. Figure 13 shows the radiative heatings in the IAP and CAM3.1 models with full physics and their differences . It is seen that the IAP model has larger radiative cooling in the troposphere from 700 mb to 300 mb, with thepattern of difference in Figure 13c to be similar to the pattern of temperature difference in Figure 1c. This suggests that the different radiative cooling may the major reason for different simulated temperature in the two moist models.

The variables that we used to calculate the radiative heating include temperature, clouds and water vapor. To investigate which of the variables is dominant to cause the different radiative heating between the two models, we carried out a series of offline radiation calculations [?]. The set of calculations is listed in Table 2. For simplicity, we used the annual mean from climate simulation from the two moist models in the offline calculations. Figure 14a gives radiative heating difference between the IAP_ctrl and the CAM_ctrl. There is a larger radiative cooling in most region of troposphere in IAP moist model compared to CAM moist model. The pattern of this cooling area is qualitatively the same as that in Figure 13c; the exact agreement is not expected since only annual mean fields are used. Figure 14b shows the difference of heating rate due to change of clouds. It is seen that cloud fraction is the dominant contributor to the different radiative cooling between the two moist modelsTemperature and water vapor have much smaller contributions (Fig. 14c, d). The cloud fractions in the two moist models and their differences are given in Figure 15. The IAP model simulated less high clouds (Figure 15c), and thus less greenhouse effect of clouds (Figure 14b) in the upper troposphere, leading to larger radiative cooling and colder troposphere The cause of the smaller cloud amount in

the upper troposphere is presumably due to the less energetic eddy activities, but the interactions are complicated and need further study.

4. Summary

The zonal mean temperature, zonal wind and eddy fluxes with the IAP AGCM4.0 and CAM3.1 are evaluated against the NCEP reanalysis data. The results reveal that the tropical tropospheric temperature in the IAP AGCM4.0 simulation is colder than that in the CAM3.1, but closer to NCEP reanalysis. The model also simulated a better distribution of the westerly jets. Since the main difference of the two models is the dynamical core, we used the idealized H-S test to investigate the direct impact of the dynamical cores. We showed that the IAP AGCM4.0 simulated a warmer troposphere in H-S test than the CAM3.1, which is nearly opposite to that in the full model. We carried out aqua-planet experiments to rule out the impact of different treatment of topography as the cause of the difference in the full models.

We used transformed Eulerian mean diagnostics to show that wave activities are weaker in the IAP AGCM4.0 regardless of whether moisture physics is included or not, a consequence of the more diffusive numerical scheme and less energetic eddies. In the dry model, the weaker eddies forced a reduced residual circulation in each hemisphere that can explain the warming in the IAP model. In the moist model, however, the residual circulation is in balance with the diabatic heating from physical parameterizationsThere is larger radiative cooling in the IAP model, owing to smaller cloud amount in the upper troposphere and weaker greenhouse effects of clouds. This explains the colder troposphere in the IAP model with full physics than that in the CAM model.

Our study demonstrates how interactive moist physics, especially clouds, can change the behavior of a dynamical core in climate models. It points to the need to understand dynamical cores both in isolation and with full physics. To our knowledge, this is the first effort to report and analyze the cause of the opposite impact of dynamical core between dry and moist models on climate simulation. Future research will focus on the impact of dynamical core on high latitude and stratospheric climate, and on the mechanism of cloud responses.

Acknowledgments. We wish to thank Dr. Wuyin Lin for his help and discussion in the

course of this study. This research was supported by National Basic Research Program of China (973 Program) under Grant Nos. 2010CB951901 as well as the National Natural Science Foundation of China under Grant Nos. 41005054 and 40830103 . Additional support is from the Climate Change and Prediction Program of the US Department of Energy, and the Modeling and Analysis Program of the National Administration for Space Studies to the Stony Brook University. Part of this research was carried out while the first author visited the Institute for Terrestrial and Planetary Atmosphere of the Stony brook University.

Reference:

Andrews, D. G., and McIntyre, 1976: Planetary waves in horizontal and vertical shear: The generalized Eliassen-Palm relation and the mean zonal acceleration. *J. Atmos. Sci.*, **33**, 2031-2048.

Bi, X., 1993: IAP 9L AGCM and climate simulation. Ph. D. dissertation (in Chinese), Institute of Atmospheric Physics, Chinese Academy of Sciences, 210 pp.

Boer, G. J., and coauthors, 1992: Some results from an intercomparison of the climates simulated by 14 atmospheric general circulation models. *J. Geophys. Res.*, **97**, 12771–12786.

Boer, G. J., and B. Denis, 1997: Numerical convergence of the dynamics of a GCM. *Climate. Dyn.*, **13**, 359-374.

Chen, H., Z. Lin, and G. Zhou, 2004: Experimental dynamical prediction of spring dust storm events in China. *Climatic and Environmental Research* (in Chinese), **9**, 182-190.

Chen, M., R. B. Rood, and L. L. Takacs, 1997: Impact of a semi-Lagrangian and an Eulerian dynamical core on climate simulation. *J. Climate*, **10**, 2374-2389.

Collins, W. D., and coauthors, 2004: Description of the NCAR community atmosphere model (CAM3.0). NCAR Technical Note NCAR/TN-464+STR, xii+214 pp.

Held, I. M., and M. J. Suarez, 1994: A proposal for the intercomparison of the dynamical cores of atmospheric general circulation models. *Bull. Amer. Meteor. Soc.*, **75**, 1825-1830.

Holton, J. R., 2004: An introduction to dynamic meteorology. International Geophysical Series, Vol. 88, 4 ed., Academic Press, 535 pp.

Hurrell, J. W., J. J. Hack, A. S. Phillips, J. Caron, and J. Yin, 2006: The dynamical simulation of the community atmosphere model version 3 (CAM3). *J. Climate*, **19**, 2162-2183.

Jablonowski, C., and D. L.Williamson, 2006: Baroclinic wave test case for Dynamical cores of GCMs. *Quart. J. Roy. Meteor. Soc.*, **132**, 2943-2976.

Kalnay, E., and coauthors, 1996: The NCEP/NCAR 40-year reanalysis project. *Bull. Amer. Meteor. Soc.*, **77**, 437-471.

Liang, X., 1996: Description of a nine-level grid point atmospheric general circulation model. *Adv. Atmos. Sci.*, **13**, 269-298.

Lin, Z., and Q. Zeng, 1997. Simulation of East Asian summer monsoon by using an improved AGCM. *Adv. Atmos. Sci.*, **14**, 513-526.

Lorenz, D. J., and E. T. DeWeaver, 2007: Tropopause height and zonal wind response to global warming in the IPCC scenario integrations, *J. Geophys. Res.*, **112**, D10119, doi:10.1029/2006JD008087.

Neale, R. B., and B. J. Hoskins, 2001: A standard test for AGCMs including their physical parameterizations: I: The proposal. *Atmos. Sci. Lett.*, **1**, 101-107.

Polvani, L. M., R. K. Scott, and S. J. Thomas, 2004: Numerically converged solutions of the global primitive equations for testing the dynamical core of atmospheric GCMs. *Mon. Wea. Rev.*, **132**, 2539-2552.

Rayner, N. A., and coauthors, 2003: Global analyses of sea surface temperature, sea ice, and night marine air temperature since the late nineteenth century. *J. Geophys. Res.*, **108**, 4407, doi:10.1029/2002JD002670.

Reynolds, R. W., N. A. Rayner, T. M. Smith, D. C. Stokes, and W. Wang, 2002: An improved in situ and satellite SST analysis for climate. *J. Climate*, **15**, 1609-1625.

Xue, F., X. Bi, and Y. Lin, 2001: Modelling the global monsoon system by IAP 9L AGCM. *Adv. Atmos. Sci.*, **18**, 404-412.

Wan, H., A. G. Marco, and B. Luca, 2008: Ensemble Held-Suarez test with a spectral transform model: variability, sensitivity, and convergence. *Mon. Wea. Rev*., **136**, 1075-1092.

Zeng, Q., and coauthors, 1989: Documentation of IAP Two-Level Atmospheric General Circulation Model. DOE/ER/60314-H1, TR044. 383 pp.

Zeng, Q., and coauthors, 1997: Seasonal and extraseasonal predictions of summer monsoon precipitation by GCMs. *Adv. Atmos. Sci.*, **14**, 163-176.

Zeng, Q., and M. Mu, 2002: The design of compact and internally consistent model of climate system dynamics. *Chinese J. Atmos. Sci.*, **26**: 107-113.

Zhang, H., 2009: Development of IAP atmospheric general circulation model version 4.0 and its climate simulations. Ph. D. dissertation (in Chinese), Institute of Atmospheric Physics, Chinese Academy of Sciences, 194 pp.

Zhang, H., Z. Lin, and Q. Zeng, 2009: The computational scheme and the test for dynamical framework of IAP AGCM-4. *Chinese Journal of Atmospheric Sciences*(in Chinese), **33**, 1267-1285.

Zhang, H., Z. Lin, and Q. Zeng, 2010: The mutual response between dynamical core and physical parameterizations in atmospheric general circulation models. *Climatic and Environmental Research*(in Chinese), **15**, (in press).

Zuo, R., 2003: Development of new generation grid point atmospheric general circulation model with high resolution. Ph. D. dissertation (in Chinese), PLA University of Science and Technology, 328 pp.

Tables

Table 1. Correlation coefficients of adiabatic heating, diabatic heating and total heating in climate simulation and H-S test by the IAP model.

	correlation coefficients		
	adiabatic heating .vs. total heating	diabatic heating .vs. total heating	adiabatic heating .vs. diabatic heating
climate simulation	0.445	0.443	-0.603
H-S test	0.947	0.132	-0.191

Table 2. Design of offline radiation calculations, the fields with suffix ‘CAM’ are from climate simulation of CAM, while the fields with suffix ‘IAP’ are from climate simulation of IAP

Experiment Name	**Sensitive Fields**		
	Temperature	**Specific Humidity**	**Cloud Fraction**
CAM_ctrl	T_CAM	Q_CAM	CLD_CAM

IAP_ctrl	T_IAP	Q_IAP	CLD_IAP
IAP_CLDonly	T_CAM	Q_CAM	CLD_IAP
IAP_Tonly	T_IAP	Q_CAM	CLD_CAM
IAP_Qonly	T_CAM	Q_IAP	CLD_CAM

Figures

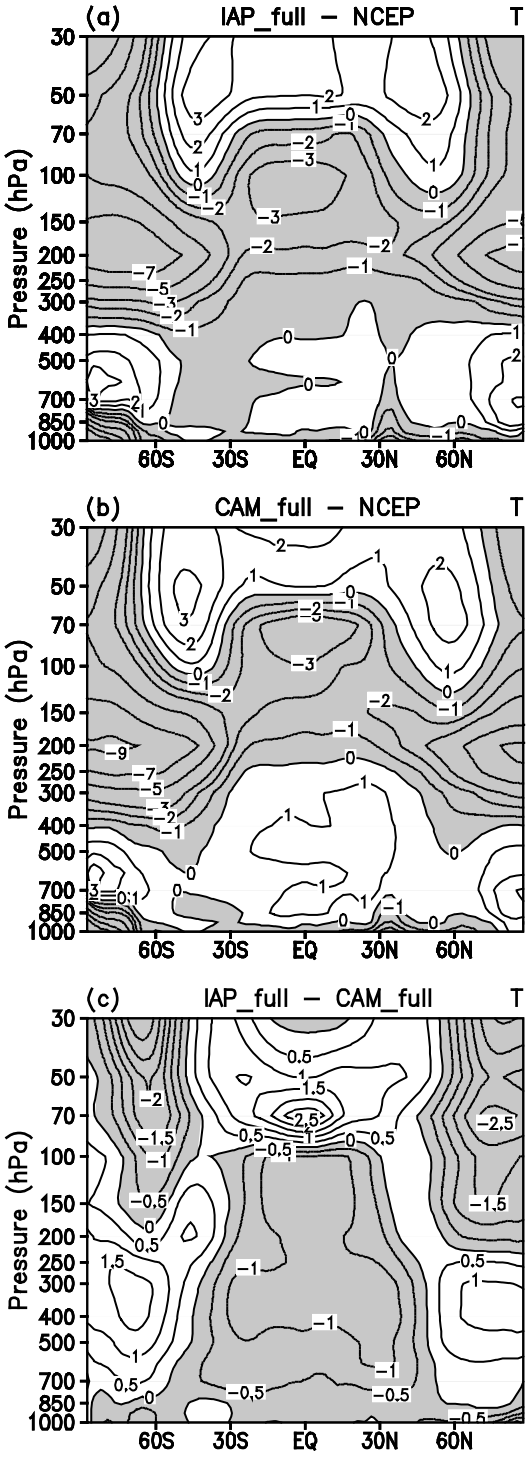

Fig.1. The biases of zonally averaged annual mean temperature from (a) IAP and (b) CAM simulations with contrast to NCEP reanalysis data, and (c) their difference (IAP - CAM). Counter intervals are 1 K in (a) and (b) and 0.5 K in (c), and negative values are shaded.

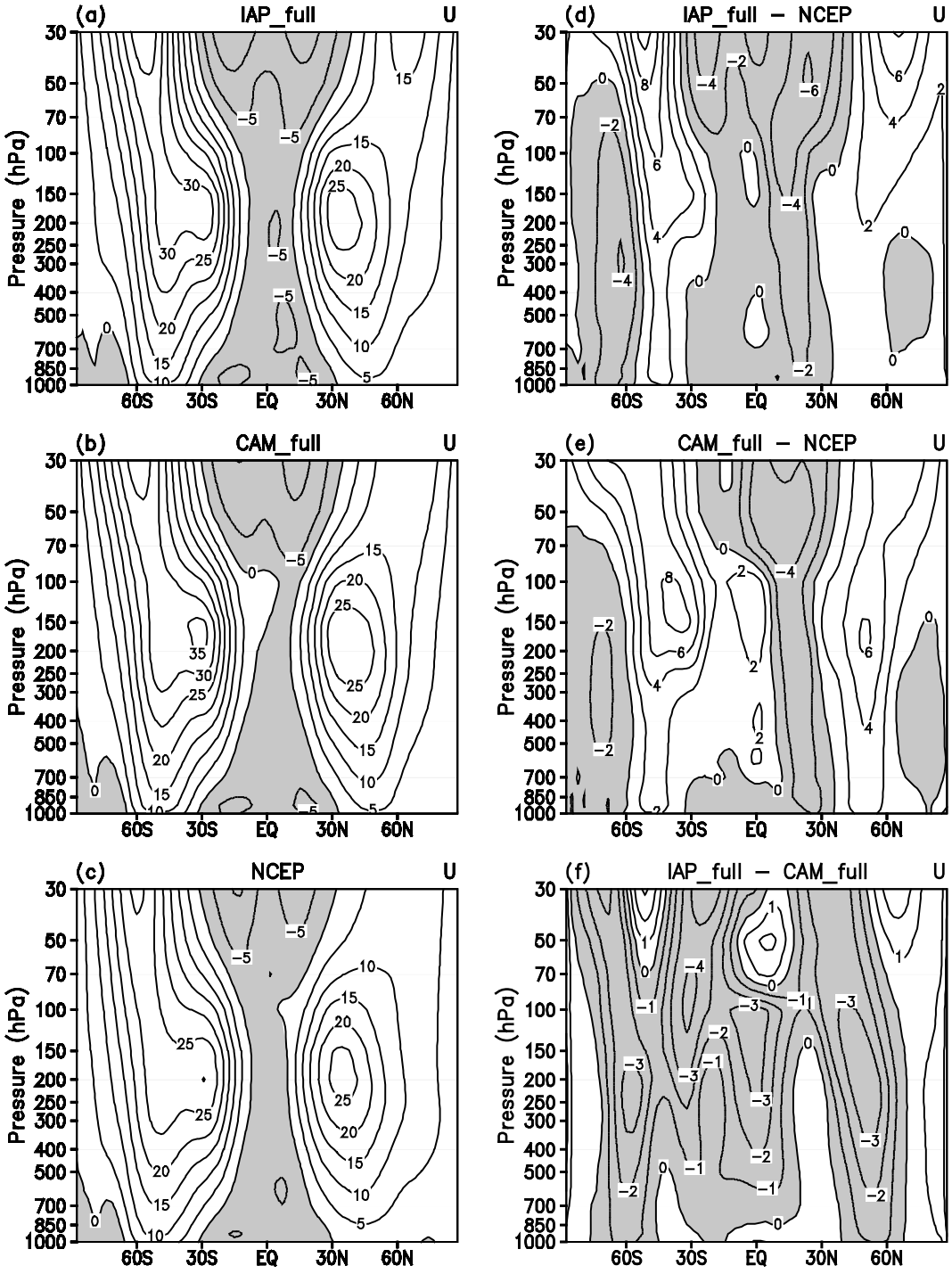

Fig. 2. Zonally averaged annual mean zonal wind from (a) IAP , (b) CAM, (c) NCEP reanalysis data, the biases of (d) IAP and (e) CAM with contrast to NCEP reanalysis data, and (f) the difference of the two simulations (IAP - CAM). Counter intervals are 5 m s^{-1} in (a), (b) and (c), 2 m s^{-1} in (d) and (e), and 1 m s^{-1} in (f). Negative values are shaded.

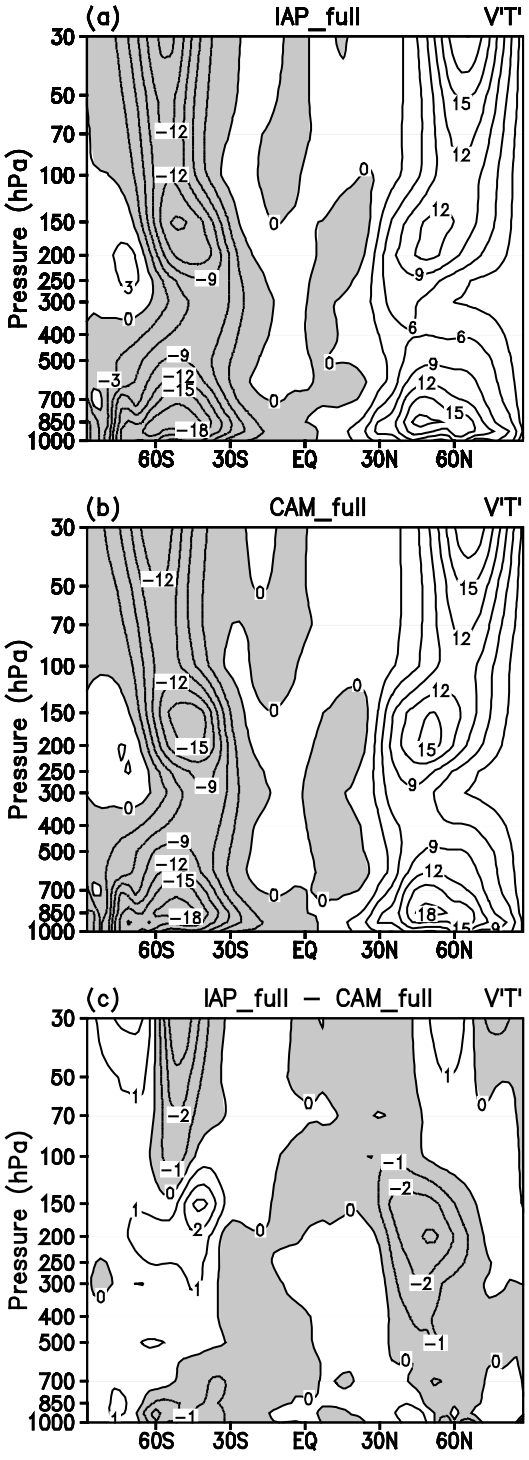

Fig. 3. Zonally averaged annual mean transient eddy heat flux from (a) IAP and (b) CAM simulations, and (c) their difference (IAP - CAM). Counter intervals are 3 K m s-1 in (a) and (b), 1 K m s-1 in (c) and negative values are shaded.

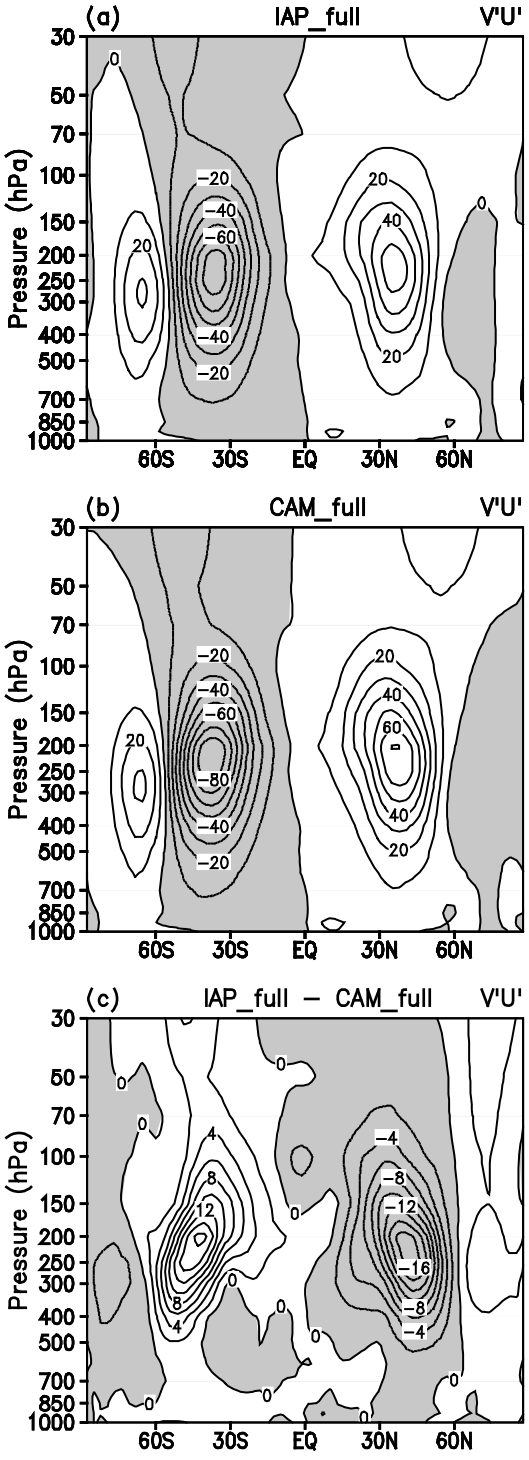

Fig. 4. Same as Fig. 3, but for transient eddy momentum flux. Counter intervals are 10 $m^2 s^{-2}$ in (a) and (b), 2 $m^2 s^{-1}$ in (c) and negative values are shaded.

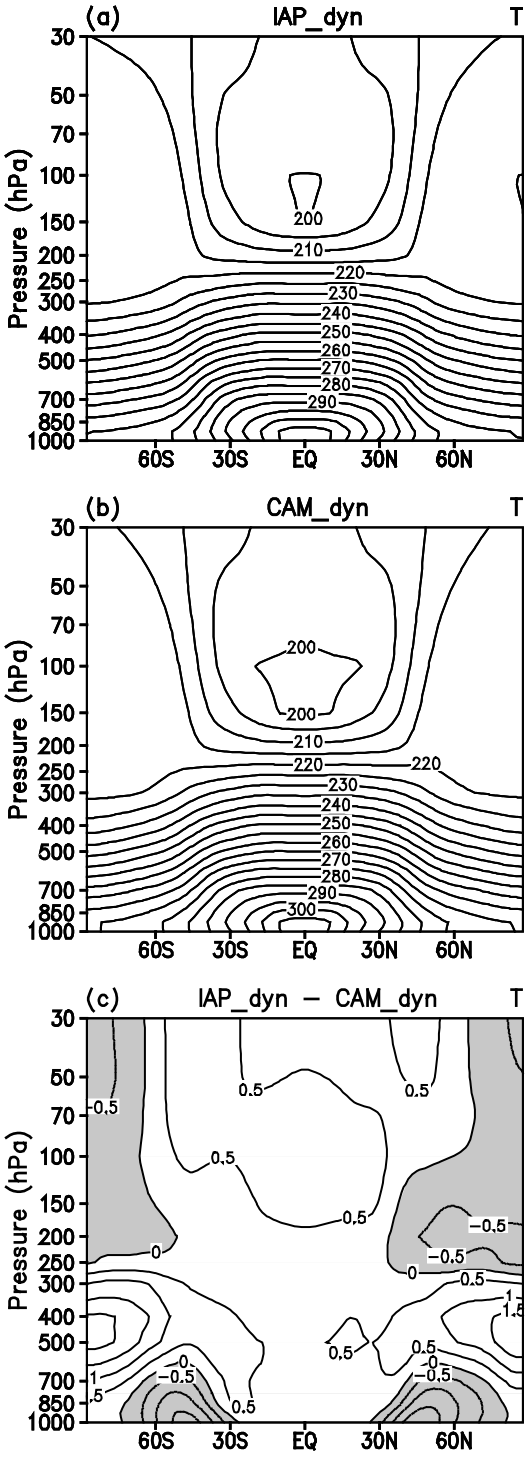

Fig. 5. Zonally averaged 1000-day mean temperature from the Held-Suarez tests with the (a) IAP and (b) CAM dynamical cores, and (c) their difference (IAP - CAM). Counter intervals are 5 K in (a) and (b), 0.5 K in (c) and negative values are shaded.

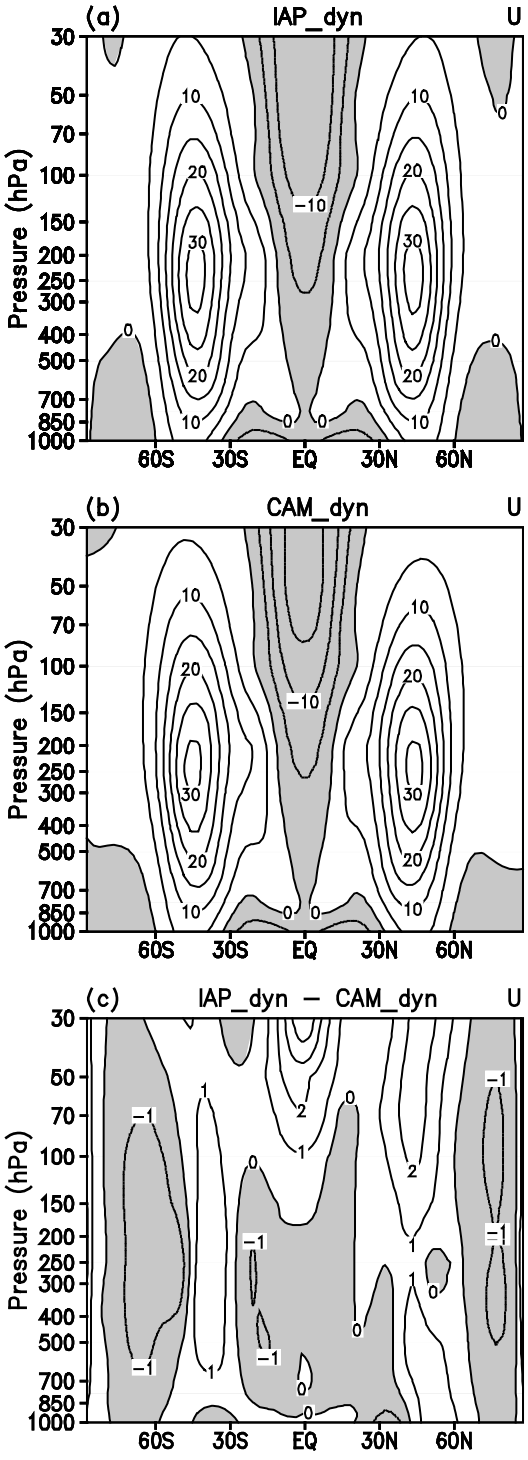

Fig. 6. Same as Fig. 5, but for zonal wind. Counter intervals are 5 m s^{-1} in (a) and (b), 1 m s^{-1} in (c) and negative values are shaded.

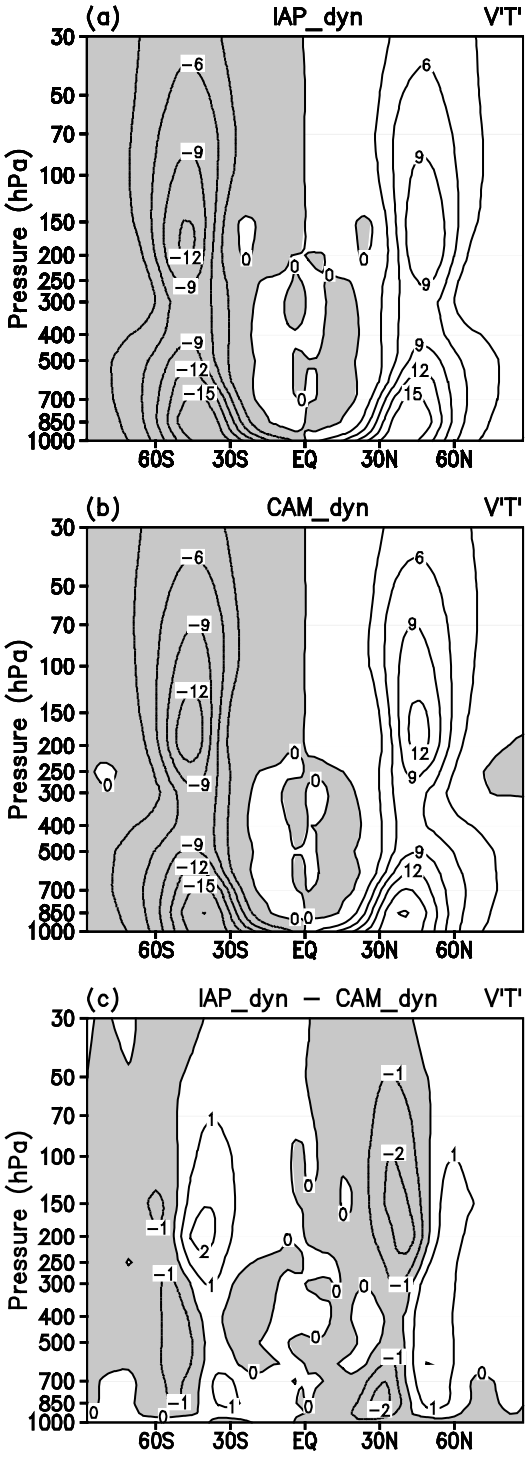

Fig. 7. Same as Fig. 5, but for transient eddy heat flux. Counter intervals are 3 K m s^{-1} in (a) and (b), 1 K m s^{-1} in (c) and negative values are shaded.

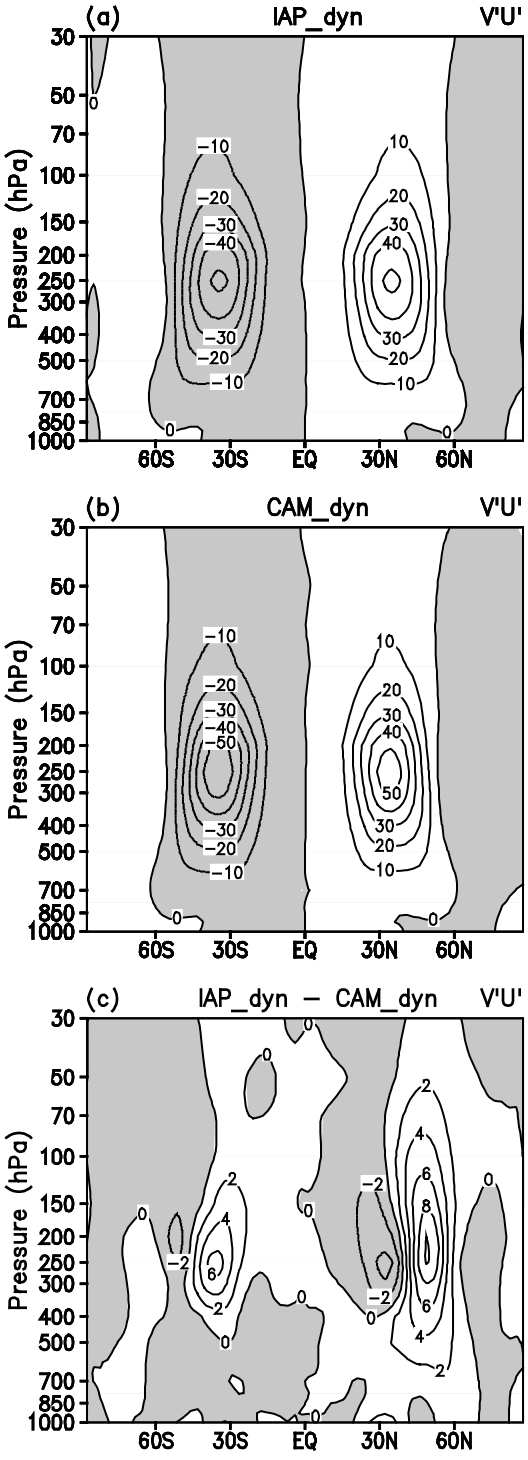

Fig. 8. Same as Fig. 5, but for transient eddy momentum flux. Counter intervals are 10 $m^2 s^{-2}$ in (a) and (b), and 2 $m^2 s^{-2}$ in (c).

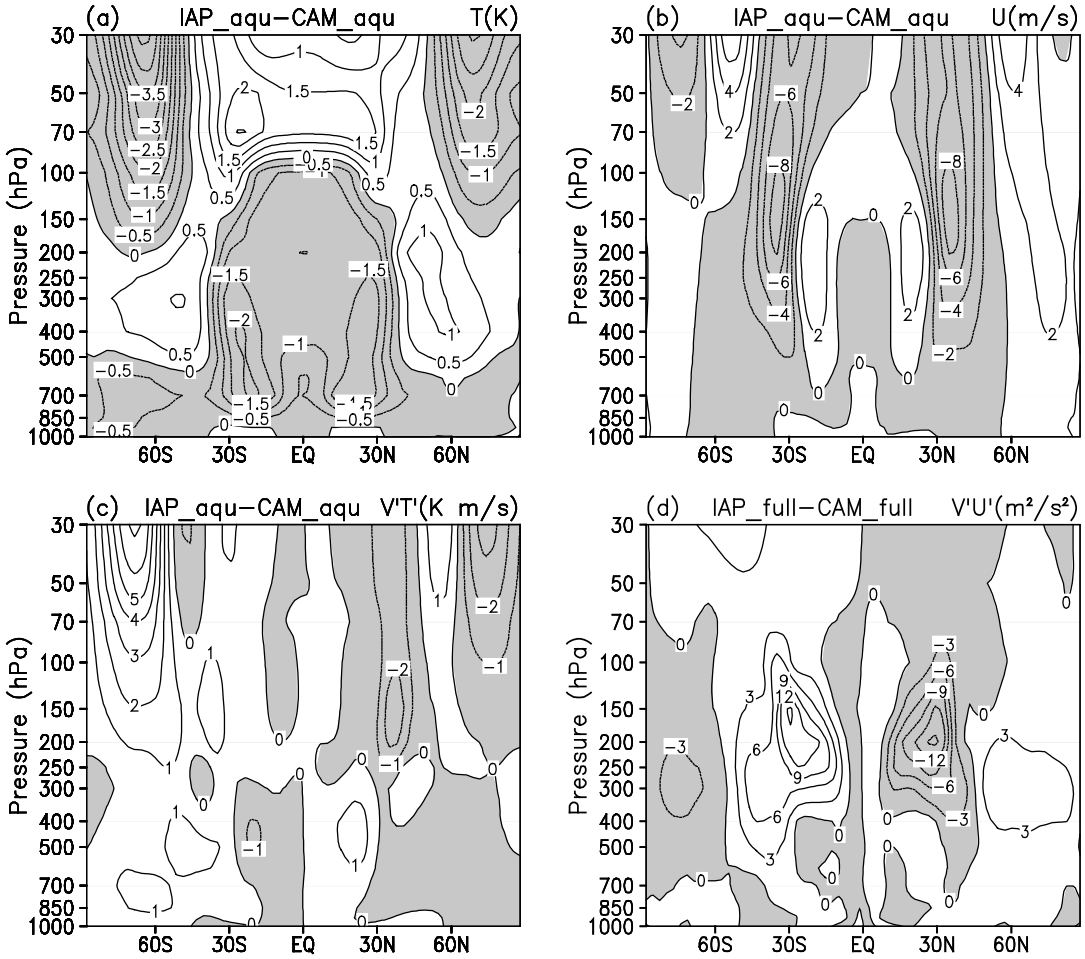

Fig. 9. The difference of zonally averaged annual mean between IAP and CAM from aqua planet tests: (a) temperature; (b) zonal wind; (c) transient eddy heat flux; (d) transient eddy momentum flux. Counter intervals are 0.5 K in (a), 2 m s^{-1} in (b), 1 K m s^{-1} in (c), 3 m^2 s^{-2} in (d), and negative values are shaded.

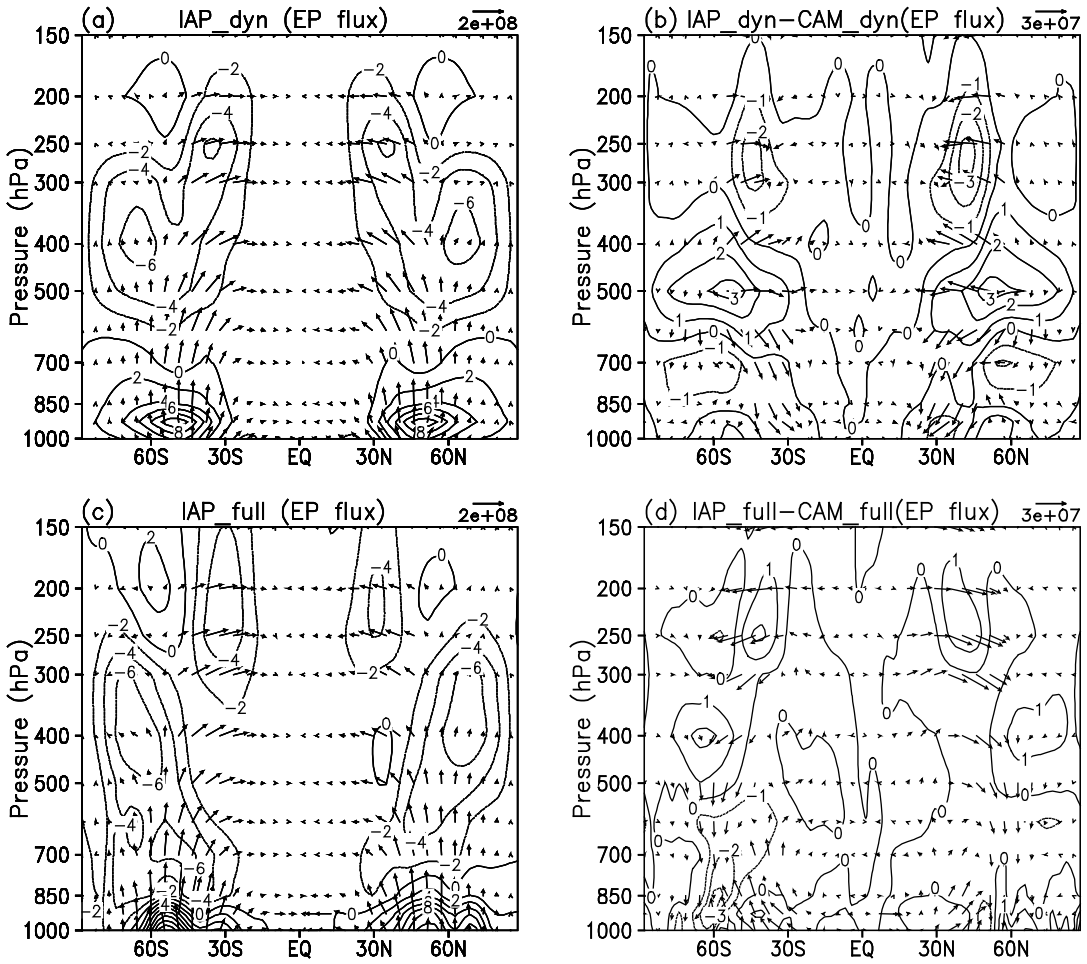

Fig. 10. Vector EP flux and its divergence from the Held-Suarez tests with the (a) IAP and (b) differences between IAP and CAM dynamical cores (IAP - CAM), and from climate simulations from (c) IAP AGCM4.0 and (d) differences between IAP AGCM4.0 and CAM3.1 (IAP AGCM4.0 – CAM3.1). Contour intervals are 2 m s^{-1} day^{-1} in (a) and (c), and 1 m s^{-1} day^{-1} in (b) and (d). The flux is in the unit of kg s^{-2}. The vertical component of the flux is multiplied by a factor of 100 to make proper vector plots.

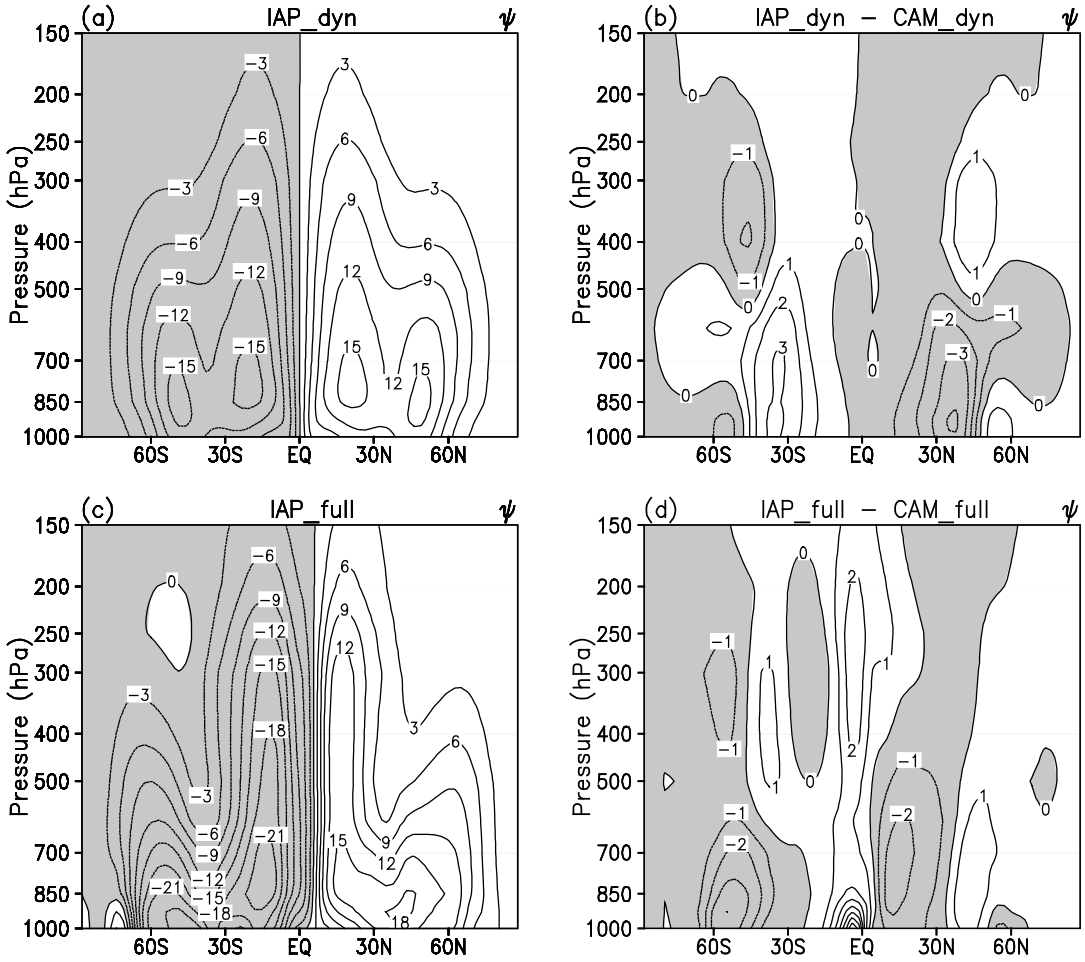

Fig. 11. Same as Fig. 9, but for meridional stream function of residual circulation. Contour intervals are $3x10^2$ kg m^{-1} s^{-1} in (a) and (c), and $1x10^2$ kg m^{-1} s^{-1} in (b) and (d).

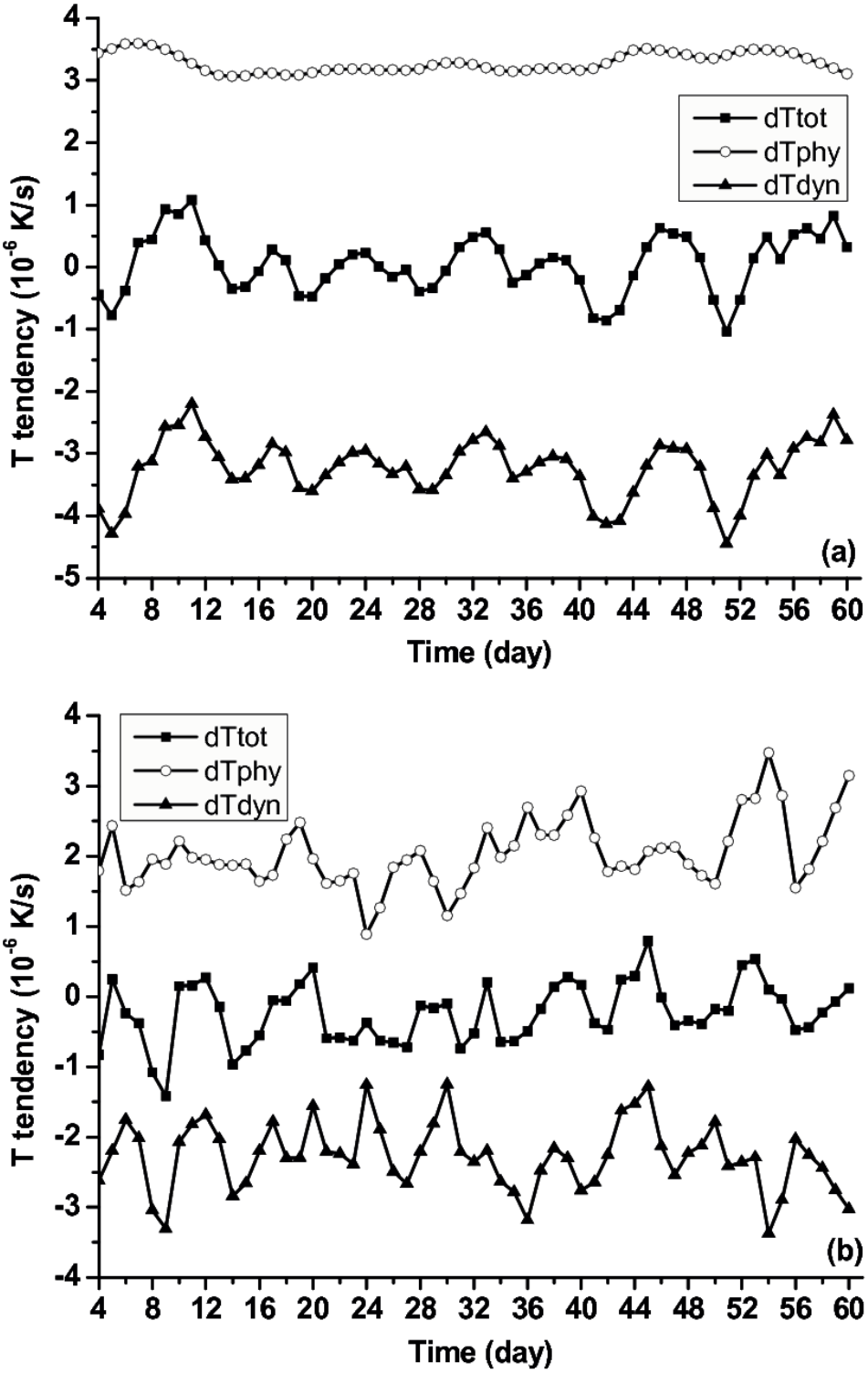

Fig. 12. Evolution of heating rate from IAP model in (a) Held-Suarez test and (b) climate simulation in troposphere (150 hPa – 1000 hPa) at low latitude (30°S - 30°N). Solid square: diabatic heating rate, solid triangle: adiabatic heating rate, hollow circle: total heating rate. Unit: 10^6 K s^{-1}

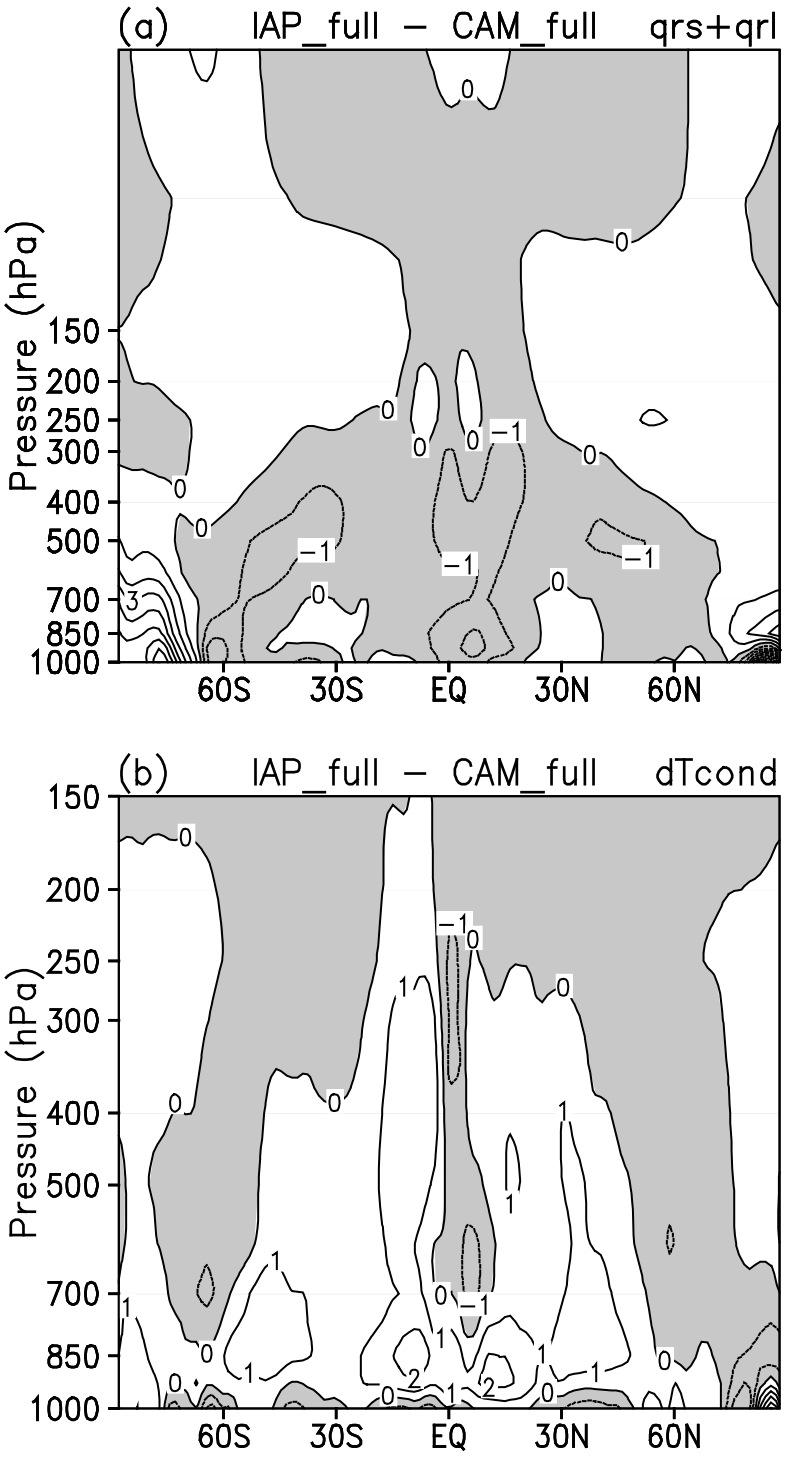

Fig. 13. Differences of simulated diabatic heating rate due to (a) radiative processes and (b) moist processes between IAP AGCM4.0 and CAM3.1 (IAP AGCM4.0 - CAM3.1). Contour intervals are 1 K day^{-1} and negative values are shaded.

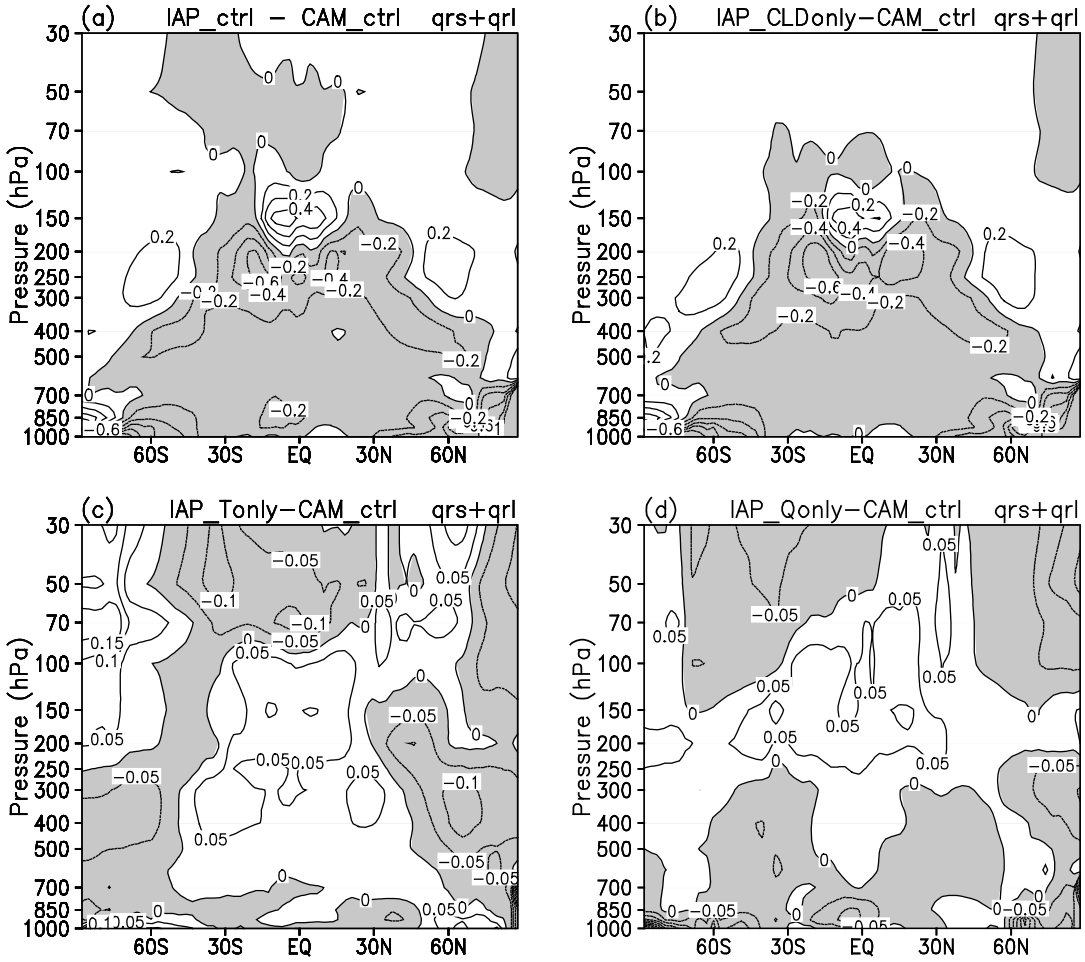

Fig. 14. Differences of radiative diabatic heating rate from the sensitive experiments: (a) IAP_ctrl − CAM_ctrl, (b) IAP_CLDonly − CAM_ctrl, (c) IAP_Tonly − CAM_ctrl, (d) IAP_Qonly − CAM_ctrl. Contour intervals are 0.2 K day^{-1} in (a) an (b), 0.05 K day^{-1} in (c) an (d), and negative values are shaded.

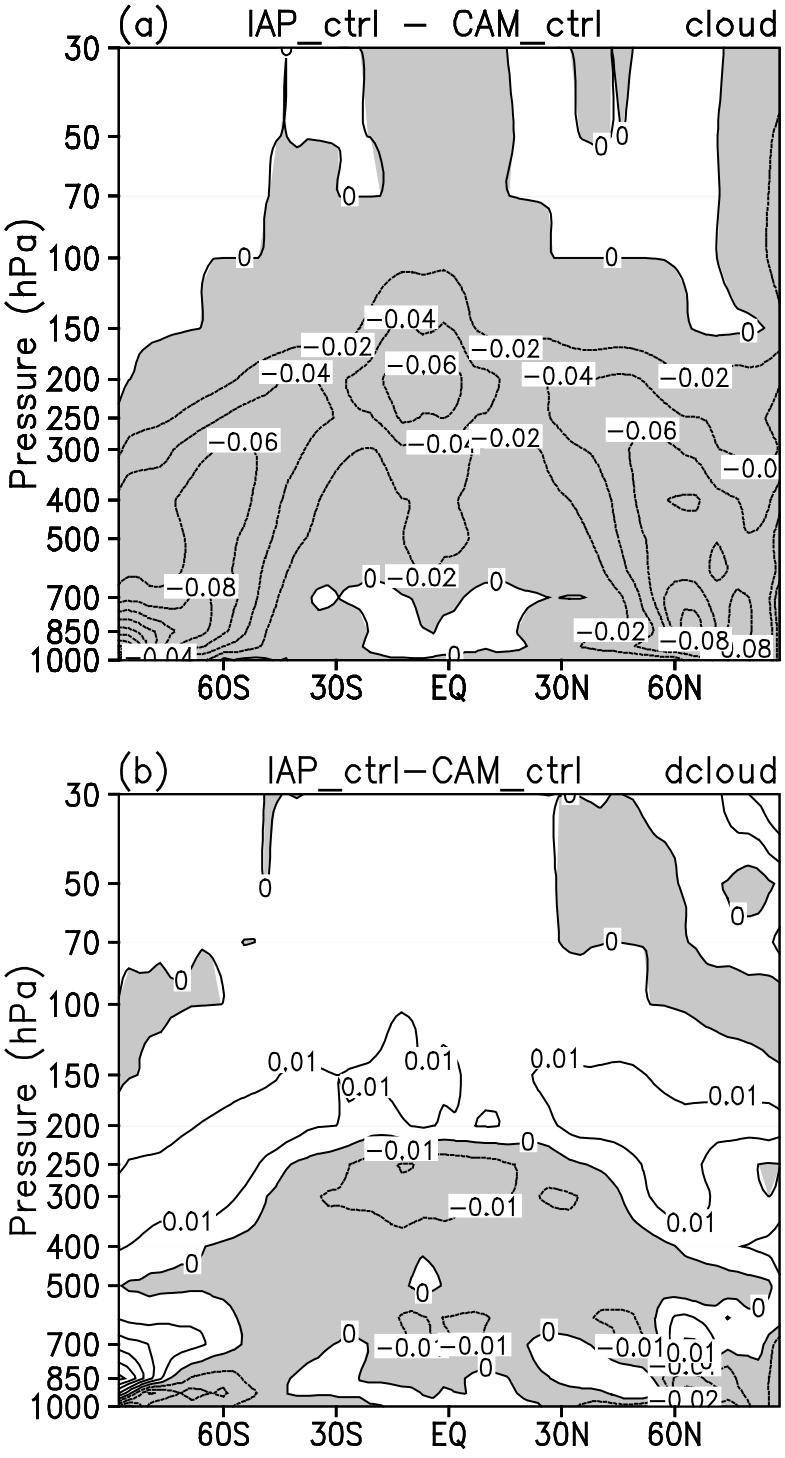

Fig. 15. Differences of simulated cloud fraction and its vertical gradient (up layer minus bottom layer) between experiments IAP_ctrl and CAM_ctrl (IAP_ctrl - CAM_ctrl). Contour values are 0.02 in (a) and 0.01 in (b), and negative values are shaded.